Simulation of convective flow and thermal conditions during ultrasonic treatment of an Al-2Cu alloy

Gui Wang[1,2], Paul Croaker[3], Matthew Dargusch[1,2], Damian McGuckin[4], David StJohn[1,2]

[1]Defence Materials Technology Centre (DMTC), The University of Queensland, St Lucia QLD 4072 Australia

[2]Centre for Advanced Materials Processing and Manufacturing, The University of Queensland, St Lucia, Queensland, 4072, Australia

[3]School of Mechanical and Manufacturing Engineering, University of New South Wales, Kensington NSW 2033 Australia

[4]Pacific Engineering Systems International, Glebe, NSW 2037 Australia

Abstract

Grain refinement of an Al-2Cu alloy using ultrasonic treatment was investigated numerically. A finite element model coupling fluid flow and heat transfer was developed and validated by comparing the results of both numerical simulations and physical experiments. The model successfully describes hydrodynamic fields generated by ultrasonic treatment and its influence on heat transfer. The simulations were used to study the influence of the duration of ultrasonic treatment and the associated acoustic streaming on convection and the resulting temperature distribution. It was revealed that a relatively cold sonotrode applied during ultrasonic treatment for up to 4 minutes created a casting environment that promoted crystal nucleation and enabled their growth and survival during transport of these grains into the bulk of the melt by strong convection. The enhanced convection established a low temperature gradient throughout the melt which favours the formation of an equiaxed grain structure. Therefore, the convection induced by acoustic streaming plays a critical role in facilitating nucleation, growth, and transport of grains.

Keywords: Aluminium alloy; Grain refinement; Acoustic streaming; Solidification.

1. Introduction

The formation of the as-cast structure of metallic alloys is controlled by the nucleation, growth and transport of grains within the melt, which in turn is affected by heat and solute diffusion and convection which also control the morphology of crystals [1]. By controlling the nucleation and the growth processes, the as-cast grain structure of alloys can be modified to promote nucleation and restrict grain growth producing a refined structure.

It is well known that vibration induced ultrasonically, mechanically or electromagnetically, can cause grain refinement that is similar to or better than chemical nucleation [1-4]. Ultrasonic vibration characterised by high-intensity and low-amplitude is one of the physical/mechanical means that have been demonstrated to refine the as-cast grain structure without using inoculant particles [5-8]. Decades of research have revealed that UltraSonic Treatment (UST) is a potentially efficient, clean and versatile technology. However, UST is still mostly confined to

the laboratory. There has been limited industrial application due to a lack of understanding of the interactions between the ultrasonic field, the subsequently generated flow in the molten metal, and solidification [9]. Hence, the development of computational models that quantitatively describe hydrodynamic fields induced by ultrasonics are needed in order to understand and optimise UST processes.

The basis of ultrasonic processing is the formation of cavitation bubbles, their pulsation and collapse in melts subjected to high-frequency, high-power vibrations, and the resulting acoustic streaming that extends the influence of ultrasound to a larger melt volume [10]. It has been proposed that nucleation due to cavitation is caused by some mix of (1) an increase in the melting point and thus undercooling of the surrounding liquid [11] and (2) an improved wetting of the insoluble inclusions by the melt [12]. The undercooling of the first mechanism occurs because of the increased pressure when bubbles collapse and, therefore, enhanced nucleation can be expected [11]. The increased wetting of the second mechanism combines with substrate activation, in which an inert particle (like an oxide, carbide or boride) floating in the melt becomes an active substrate through the physical action of cavitation. The expansion and collapse of cavitation bubbles produce melt jets and surges of high pressure and temperature that strip the particles of absorbed gas and facilitate filling of the surface defects with liquid aluminium – the so called sono-capillary effect [5-6, 9].

Another mechanism that may occur is the detachment of crystals that nucleate directly on the sonotrode surface [12, 13]. When a cold sonotrode is immersed into the melt, there is a significant temperature drop that initiates solidification on the sonotrode surface. Depending on the condition of the surrounding melt and the sonotrode surface, the solidified grains will either remelt, continue to grow, or be detached and swept into the bulk of the melt. The grains formed on the radiating face of the sonotrode will be subjected to alternating tensile and compressive loads due to vibration at the rate of the ultrasonic frequency possibly facilitating detachment. Further, instantaneous fluctuations of pressure and temperature due to cavitation may affect grain stability on the sonotrode surface. These fluctuations may cause a repeating cycle of nucleation, growth and detachment of crystals from the radiating surface of the sonotrode. The released grains or fragments would then be transported by acoustic streaming into the rest of the melt. The mechanism of detachment may be similar to that of the fragmentation of dendritic grains which has been proposed as an important contributor to grain refinement by UST [5].

It is well known that ultrasound propagating through a viscous fluid can induce a mass flow known as acoustic streaming. This phenomenon can in general be regarded as any flow generated by the force arising from the presence of a gradient in the time-averaged acoustic momentum flux in a fluid [14]. More strictly, it is described as the time averaged flow circulating near a vibrating surface which is attributed to the friction at a solid boundary that is vibrating and in contact with a fluid [15], or the steady flow in a fluid driven by the absorption of high amplitude acoustic oscillations during the passage of an acoustic wave. The latter is called “quartz wind” because it was observed when ultrasound piezoelectric quartz came into use [16-18]. Acoustic streaming is a steady flow of fluid formed by viscous attenuation of an

acoustic wave. Using these concepts, Lighthill derived a Navier–Stokes based equation describing acoustic streaming as a non-oscillatory Reynolds stress, i.e. a time-averaged momentum flux in a fluid generated by the presence of a spatial gradient in the oscillatory Reynolds stress [14]. This approach provided a sound theoretical basic with which to model acoustic streaming under ultrasonic fields.

Computational modelling is a good way to explore the physics involved in UST [19-21], even if the widely separated time and length scales have made UST simulation impractical due to the significant computing resources and time required. In this paper, a computational model is presented that simulates acoustic streaming induced by a sonotrode by simplifying the interface between the sonotrode and the melt with the introduction of a momentum source over a volume which equals the cavitation zone. The model is based on Lighthill's acoustic streaming theory [22], and assumes that all the acoustic energy absorbed by the liquid is converted into turbulent motion, forming a jet under the sonotrode tip. Using this assumption, the Navier-Stokes equations were solved using a ESI Group's ProCAST virtual casting software [23], to determine the hydrodynamic field in the melt. The model was validated subsequently by comparing the results from computational simulations against obtained from experiments.

2. Experimental procedures

Four kilogram batches of Al–2wt%Cu alloy (Al-2Cu) were melted in an electric furnace from commercially pure aluminium (99.7%) and pure copper (99.9%).

The ultrasonic device used in this work consisted of a 2 kW commercial ultrasound generator, an air cooled 20 kHz transducer, and a sonotrode made of molybdenum based alloy with a tip 18 mm in diameter. About 1 kg of the alloy was melted and preheated inside a graphite-clay crucible with dimensions 90 mm top diameter, 60 mm bottom diameter and 120 mm in height. When the melt temperature reached 720±5°C the crucible was transferred from the furnace to the experimental platform. When the melt temperature reached 694°C which is 40°C above the liquidus temperature of 654°C, the powered sonotrode was immersed into the melt with the radiating surface 15 mm below the top surface of the melt and left there for the following three time ranges:

Range I - the UST was terminated at 660°C
Range II – the UST was terminated at 654°C, and
Range III – the UST was terminated after 4 minutes

These three ranges are shown in Figure 1b. The procedure followed to terminate UST was to remove the sonotrode from the melt, turn off the ultrasonic power and then allow the melt to solidify.

Two K-type thermocouples were placed in the melt to one side of, and below, the sonotrode: one close to the wall of the crucible and the other a further 12.5 mm from the wall. Both thermocouples were placed 45 mm above the bottom of the crucible as indicated in Figure 1a. A data-acquisition system collected temperature data by sampling 4 readings per second.

The cast samples were vertically sectioned along the centre symmetrical axis and prepared for microscopic observation using standard metallographic techniques.

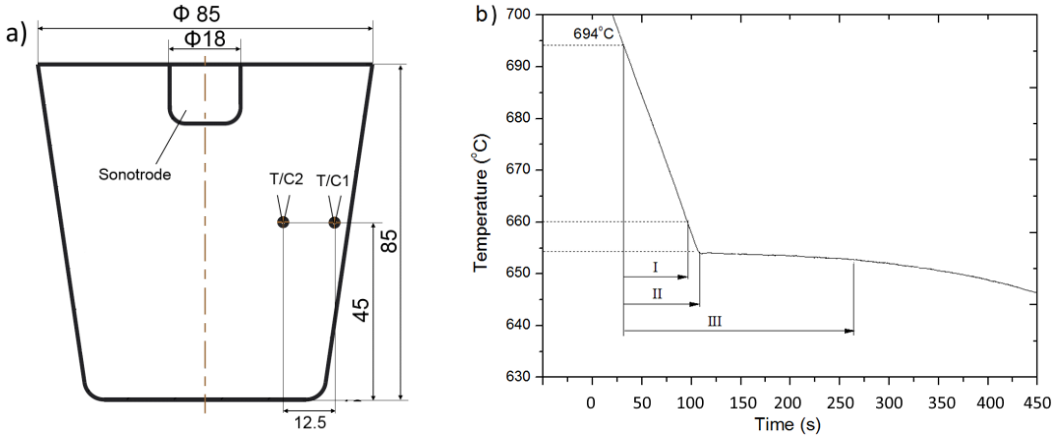

Figure 1 Schematics of (a) the cast samples indicating the locations of the ultrasonic probe (sonotrode) and thermocouples; and (b) the temperature ranges over which UST is applied: (I) from 694°C (40°C above liquidus) to 660°C (II) from 694°C to 654°C (liquidus), (III) from 694°C for 4 min to 653°C.

3. Computational model and validation

3.1 Mathematical model

The model is focused on the development of convective melt flow and its impact on the temperature distribution in a crucible similar to that used in the experiments described above. Figure 2 shows the geometric representation of the computational model and details the boundary conditions applied at the various heat exchange interfaces. The heat transfer coefficients (HTC) and the reference temperature (T_{ref}) applied at each boundary are shown in the inset table. A T_{ref} of 'Calc' indicates that ProCAST calculates the appropriate temperature based on the material temperatures adjacent to the boundary.

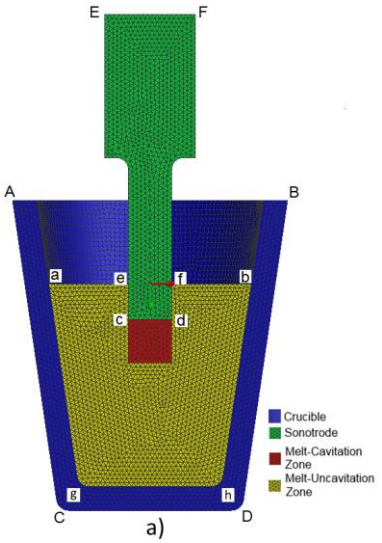

a)

Boundary	Boundary Type	HTC ($W \cdot m^{-2} °C^{-1}$)	T_{ref} (°C)
aghb	Melt-Crucible	900	Calc
AC & DB	Crucible-Air	25	20
Aa & bB	Crucible-Air	25	20
CD	Crucible-Ground	50	20
ecdf	Melt-Sonotrode	2000	Calc
Ee & fF	Sonotrode-Air	10	20
EF	Constant Temp.	-	20

b)

Figure 2 (a) Schematic diagram of casting and sonotrode geometry and (b) a table of the boundary conditions of the computational model duplicating the ultrasonic treatment condition.

The external surface of the crucible and exposed surfaces of the sonotrode and melt are air cooled, and the bottom surface of the crucible has been defined with forced cooling conditions to accommodate contact with the brick floor, as shown by section CD in Figure 2.

3.1.1 Acoustic streaming model

Acoustically induced ultrasound streaming has been modelled by assuming that the volume underneath the sonotrode tip, shown in red in Figure 2, is a source of momentum that accelerates the surrounding fluid downwards forming a jet. It is further assumed that the acoustic energy P attenuates at a constant rate per unit length r_a along the distance c, and the rate of momentum of the jet r_m equals the total acoustic momentum rate $r_a = P/c$ emitted from the acoustic power source.

Lighthill [22] calculated acoustic streaming from the Navier-stokes equation at higher Reynolds numbers by the following equation:

$$\rho(\vec{v} \cdot \nabla\vec{v}) = -\nabla p + \mu\nabla^2\vec{v} + \vec{F} \tag{1}$$

where the force F causing streaming is the spatial variation of the Reynolds stress:

$$F_j = \frac{\partial(\overline{\rho v_i v_j})}{\partial x_i} \tag{2}$$

Where power ultrasound is characterised by high intensity and a low frequency, an acoustic beam of substantial power delivers a jet at a point x_i which carries a momentum resulting in a force F_N. Assuming that the acoustic source releases its power as a narrow beam, this net force or rate of momentum at a distance X along the sound beam is defined as

$$F_N = \frac{P}{c}\left(1 - e^{-\beta X}\right) \tag{3}$$

Applying the solution for equation (1) in the case when a concentrated force $F = P/c$ is applied by an acoustic beam of power P, the kinematic momentum is:

$$K = \rho_0 F_N = \rho\frac{P}{c}\left(1 - e^{-\beta X}\right) \tag{4}$$

For the work herein, a momentum source was used to impart the force generated by the acoustic beam to the melt. The momentum source produced a total net force of about 0.024 N along the Y axis vertically across a volume of approximately 2.3E-06 m^3 located directly underneath the tip of the sonotrode.

3.1.2 Governing equations

The Al-2Cu alloy melt is incompressible and can be treated as a non-Newtonian fluid with a kinematic viscosity and a thermal diffusivity that vary with temperature. It can also be assumed that density variations of the aluminium melt are linear with respect to temperature and

restricted to the buoyancy term. The convective motion then can be modelled by the Navier–Stokes equations coupled to an energy equation as shown in Equation (5).

$$
\begin{aligned}
Mass: \quad & \frac{\partial \rho}{\partial t} + div(\rho\,\mathbf{u}) = 0 \\
x-momentum: \quad & \frac{\partial(\rho u)}{\partial t} + div(\rho u \mathbf{u}) = -\frac{\partial p}{\partial x} + div(\mu\, grad\, u) + S_{Mx} \\
y-momentum: \quad & \frac{\partial(\rho v)}{\partial t} + div(\rho v \mathbf{u}) = -\frac{\partial p}{\partial y} + div(\mu\, grad\, v) + S_{My} \\
z-momentum: \quad & \frac{\partial(\rho w)}{\partial t} + div(\rho w \mathbf{u}) = -\frac{\partial p}{\partial z} + div(\mu\, grad\, w) + S_{Mz} \\
Internal\ energy: \quad & \frac{\partial(\rho i)}{\partial t} + div(\rho i \mathbf{u}) = -\,p\, div\,\mathbf{u} + div(k\, grad\, T) + \Phi + S_i \\
Equations\ of\ state: \quad & p = p(\rho,T) \quad and \quad i = i(\rho,T)
\end{aligned}
\tag{5}
$$

In solving the governing equations using ProCAST in a three-dimensional domain, Gauss–Lobatto–Legendre point distributions were used for the spatial discretization, while a high-order splitting algorithm was used for the time discretization. A slip velocity is applied to all melt-crucible and melt-sonotrode boundaries to avoid resolving the hydrodynamics boundary layer. The slip velocity takes into account the viscous drag at the wall and the local velocity in the bulk of the flow.

3.2 Validation of the model

Time-dependent temperatures were recorded through 2 thermocouples in the experiments to be used to validate the model. As shown in Figure 3, the simulated temperatures for the case without UST (Figure 3a) and that with UST (Figure 3b) show very good agreement with the measured temperatures from the experiments.

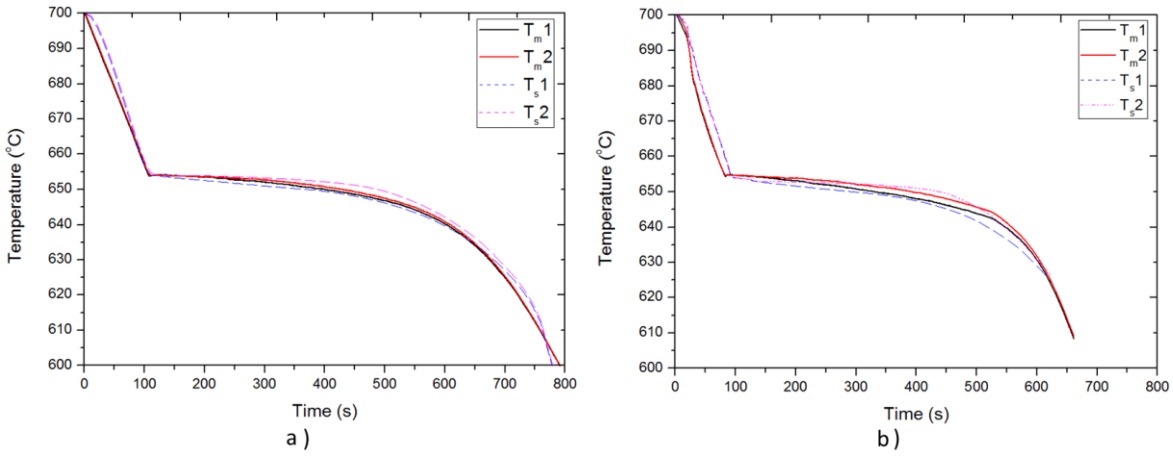

Figure 3. Cooling curves of the samples (a) without the sonotrode immersed, and (b) with UST for 4 minutes (T_m - measured temperature through experiment, and T_s - simulated temperature, T_1 and T_2 correspond to the location of the thermocouples as indicated in Figure 1a)

In particular, the current simulation results reveal that the assumption of attenuation at a constant rate, given by P/c, results in very good agreement between the simulated temperatures and those measured by the thermocouples during the experiment. This comes about because the acoustic energy P attenuates in the liquid and is converted into acoustic streaming. The assumption in the current model is that this energy is equal to the kinematic momentum k which is represented by a total net force of about 0.024 N along the Y axis vertically across a volume of approximately 2.3E-06 m^3 located directly underneath the tip of the sonotrode. In reality, a small proportion of the total energy may disperse in other directions, e.g. horizontally, which would conflict with the current assumption. However, the fact that all of the acoustic energy contributes to the forced convection, which then reduces the temperature gradient, leads to the excellent agreement achieved between the simulated temperatures and the experimental ones.

Figures 4a and 4b show respectively the magnitude of the velocity and solid fraction inside the UST. Figure $4a_1$ and $4a_2$ reveals that the flow induced underneath the radiation surface of the sonotrode produces a flow recirculation pattern. The melt flows downward to the bottom of the crucible, and then it washes the bottom and side wall. The melt then travels along the outer walls of the crucible at a lower velocity, before being swept into the region of the momentum source once again. It can also be seen that acoustic streaming results in entrainment of the liquid from the surrounding region forcing it to flow through the cavitation zone under the sonotrode. This characteristic may be advantageous for ultrasonic casting because more metal per unit time can pass through the cavitation zone. This simulated flow pattern is in agreement with water and other analogue experiments [9, 24], and the maximum velocity of 0.38 m/s is also close to the measured value reported in [25]. With an increasing solid fraction the magnitude of the velocity is dampened. For example, the maximum magnitude of the velocity is 0.38 m/s when ultrasonics is applied with a fraction solid of 0.1%, and then it drops to 0.32 m/s and 0.20 m/s when fraction solid reaches to 7.7% and 16.6% respectively. It is difficult to maintain flow when the solid fraction reaches approximately 16.6% as shown in Figure $4a_3$.

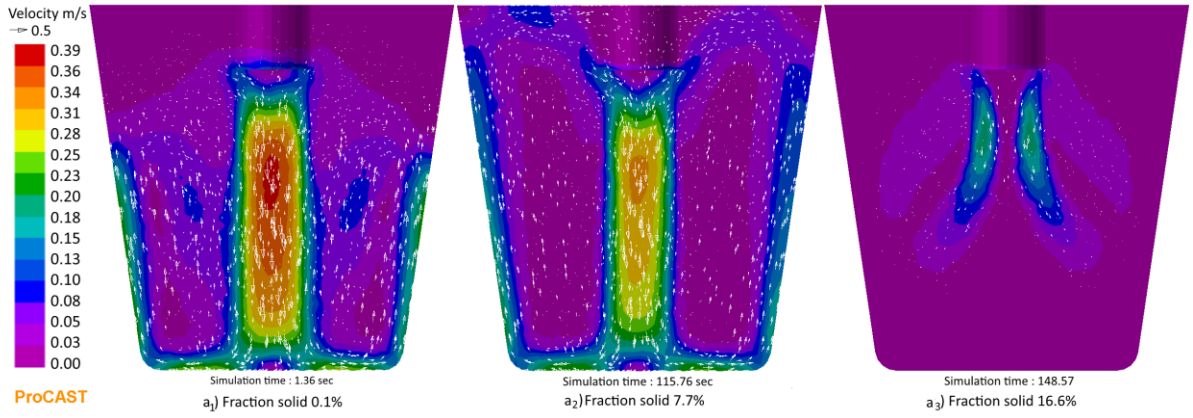

a_1) Fraction solid 0.1% a_2)Fraction solid 7.7% a_3) Fraction solid 16.6%

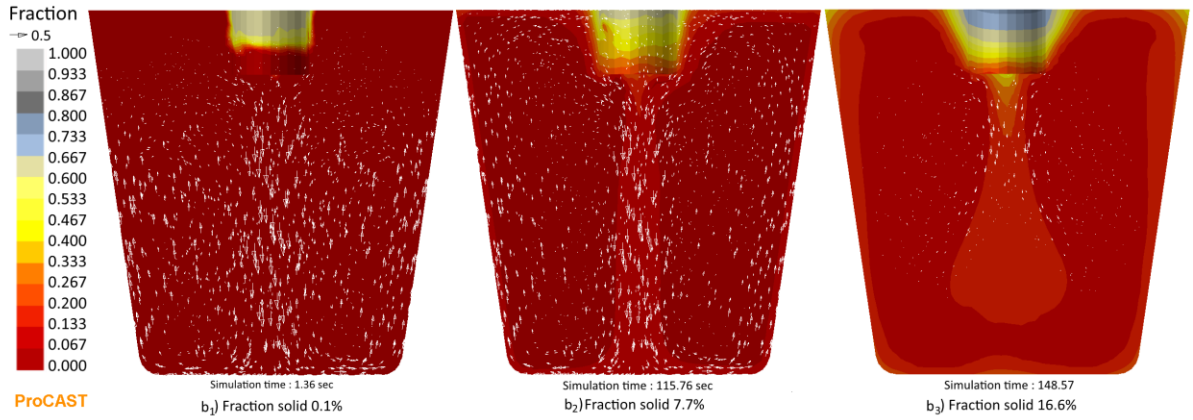

Figure 4 Simulation results of (a) fluid velocity magnitude and (b) solid fraction (1 - after 1.36 seconds and solid fraction 0.1%, 2 - after 115.76 seconds and solid fraction 7.7%, 3 - after 148.57 seconds and solid fraction 16.6%)

The solid fraction shown in Figure 4b indicates that solidification occurred on the conotrode's side wall immediately the sonotrode was immersed into the melt. However, the insignificant solidification observed on the radiation surface of the sonotrode indicates that the high level streaming on the radiation face under the sonotrode swept the chilled melt from this area and mixed this volume with the bulk of the melt. It was also found that during the entire cooling and solidification process, the sonotrode became an additional cold source chilling the melt, and the radiation surface of the sonotrode continuously sends cooler melt, or even partially solidified grains, into the bulk of the melt. Figure 4b_2 shows that a certain level of solidification occurs on the surface of the sample (the location of T/C_1) with a solid fraction of about 0.1%, with the total solid fraction reaching 7.7% at the simulation time of 115.76 seconds. The simulated temperature is slightly lower than the liquidus temperature with no obvious solid fraction in the T/C_2 location. This comes about not only because a very low volume solidifies in this region, but also because the forced convective flow mixes the solidified phase with the hotter melt, therefore, reducing the local solid fraction.

4. Results and discussion

4.1 Macrostructure of the cast samples

The macrostructures of the samples solidified without UST showing large equiaxed dendrites in the central and lower parts of the sample and columnar dendritic grains at the top is shown in Figure 5a. Applying UST produces interesting results. Terminating UST just a few degrees above the liquidus, or UST over 694-660°C, produced a macrostructure similar to that of the non-UST treated sample (Figure 5b). Terminating UST instead at the liquidus temperature, or UST over 694-654°C, produced to a combination of refined non-dendritic or less-dendritic grains in the bottom region and coarse developed dendrites in the upper region of the sample (Figure 5c). Applying UST for the 4 minutes from 694°C produced significant refinement uniformly throughout the sample (Figure 5d).

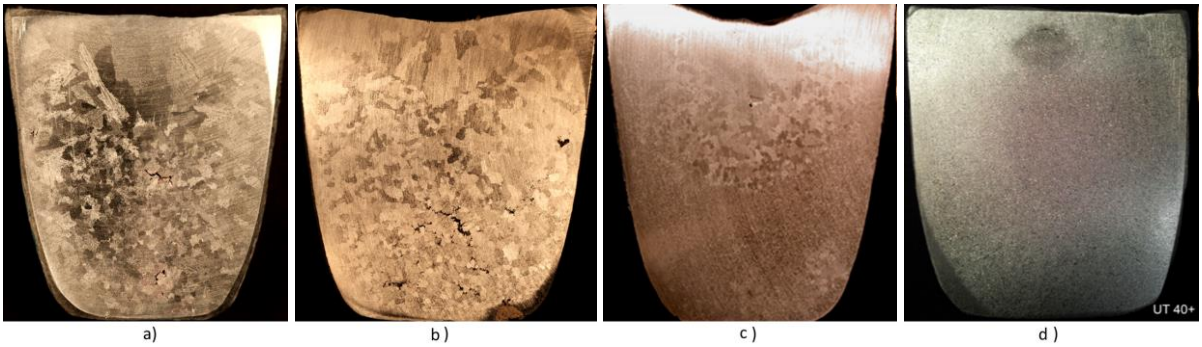

Figure 5 Macrostructure of the UST experimental specimens (a) No UST, (b) UST at 694-660°C, (c) UST 694-654°C, and (d) UST from 694°C for 4 min

4.2 Effect of the non-preheated sonotrode on the melt temperature under the sonotrode

Figure 6 shows the simulated cooling curves at three points located under the sonotrode. The locations of the three points are A, B and C depicted in Figure 6a. Figure 6b shows the cooling curves at these three points for the case when the sonotrode is not immersed in the melt. The temperature is observed to change gradually and resembles normal experimental cooling curves for aluminium alloys. The temperature for point A is slightly lower than that of points B and C and solidification occurs in the order of A, B and then C. The three points share a similar solidification time of about 740 seconds. Figure 6c represents the case when the sonotrode is immersed in the melt, but UST is not applied. The temperature at point A is observed to drop instantly by 40°C and then continues to decrease to the liquidus temperature (654°C) at a relatively slow rate. This significant reduced temperature is attributed to the localised chilling effect of the immersed sonotrode. After 20 seconds, the temperature at point A has recovered from the lowest point of 654°C to rise to 662°C. This is because the strong chilling effect from a relative small volume of the sonotrode tip is not maintained due to rapid heating of the sonotrode by the thermally conductive hot melt. However, the lower temperature at point A, compared to points B and C, for the 240 seconds that the sonotrode is immersed indicates that some chilling due to the sonotrode is maintained during nucleation and solidification. The temperature at point B dropped rapidly by approximately 20°C and then the cooling rate at this location also decreased. The temperature profile at point C reveals that the cold, stationary sonotrode has little effect on the temperature at the centre of the melt. The total solidification time when the sonotrode is immersed without activating the sonontrode, has been reduced from 740 seconds to approximately 720 seconds. This represents only a 2.7% reduction in the solidification time. This indicates that the sonotrode has a limited thermal influence throughout the melt, except for an increased cooling rate that is localized to the region surrounding the immersed sonotrode. Figure 6d shows the cooling curves for the case when the sonotrode is immersed in the melt and UST is applied. Similar to the case when UST is not applied, the initial temperature dropped instantly. However, with UST, applied the temperature recovers quite quickly and the temperature gradient reduces more rapidly due to the strong convective flow induced by the UST. The convective flow enhanced heat dispersion also reduced the total solidification time from the initial 740 seconds to 640 seconds (i.e. by 13.5%) as indicated earlier.

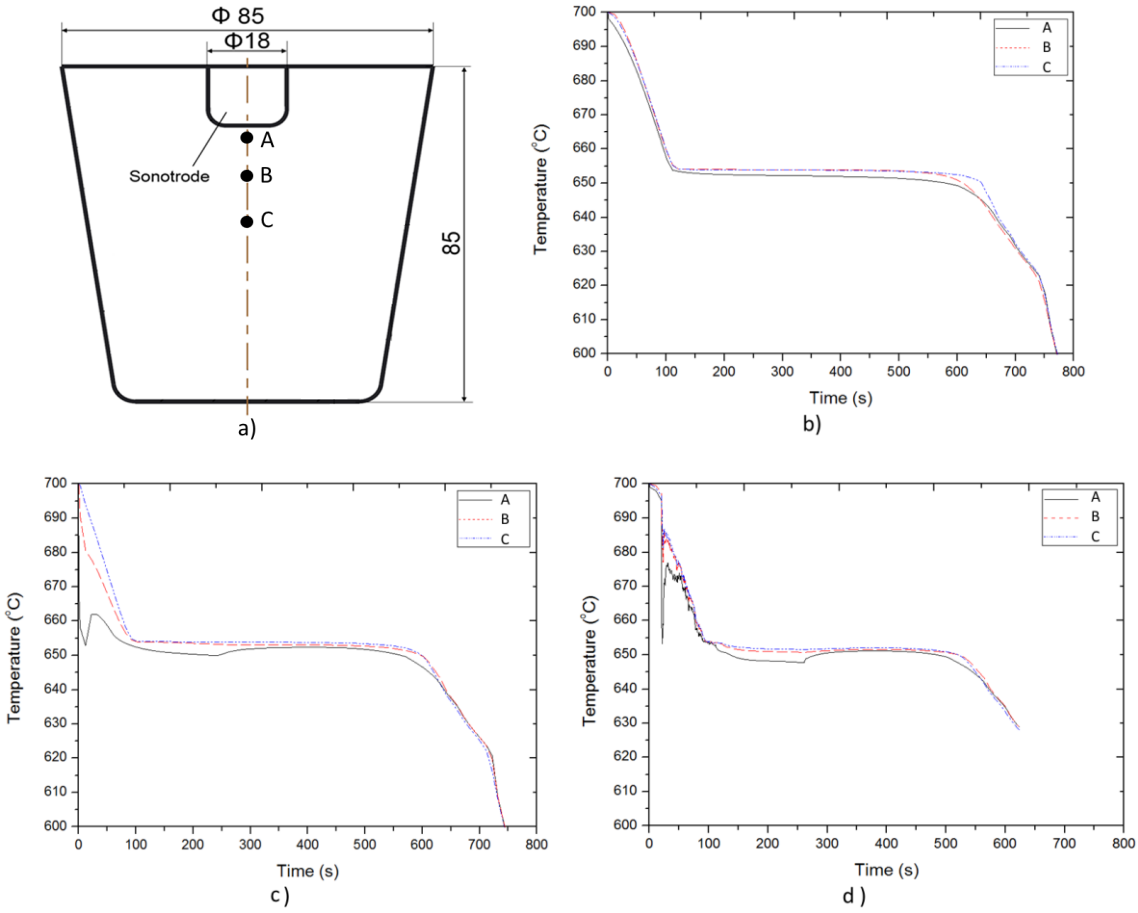

Figure 6 (a) Schematic of three points located under the sonotrode for validating the chill effect of the sonotrode on the melt; and simulated cooling curves for (b) without sonotrode, (c) no UST with immersed sonotrode, and (d) UST with immersed sonotrode.

4.3 Effect of the UST conditions on the thermal environment of the melt

Figure 7 shows simulated temperature distributions across a vertical section of the casting (a) without UST, (b) UST applied over temperature Range I (694°C to 660°C), (c) UST applied over temperature Range II (694°C to 654°C), and (d) UST applied over temperature Range III (694°C for 4 min).

Without UST, the temperature is distributed symmetrically, and the thermal contours show that the heat dissipates through the crucible wall and the top open surface. The bottom part is the coolest part of the melt followed by the top surface. Because of this type of thermal pattern, the temperature gradient from the outer surfaces to the centre can be easily established and maintained during the entire solidification process, and this kind of thermal condition can lead to a progressive solidification mode.

Conversely, with UST, the forced convection induced by acoustic streaming significantly enhanced the uniformity of the temperature distribution, and almost no obvious temperature gradient exists between the outer surfaces and the centre of the melt during the UST process. It is also noticeable that a relatively colder area exists around the vertical sides of the sonotrode indicating a chilling effect of the sonotrode and weak flow capability in the area. Figure 7b$_1$

shows the temperature field just after the sonotrode was removed from the melt when the temperature at T/C_2 reaches 660°C. It can be observed that by the time UST is terminated, the temperature was distributed uniformly throughout the melt, but the temperature gradient then increased very quickly from the outer wall to the centre as shown in Figure $7b_2$ and Figure$7b_3$.

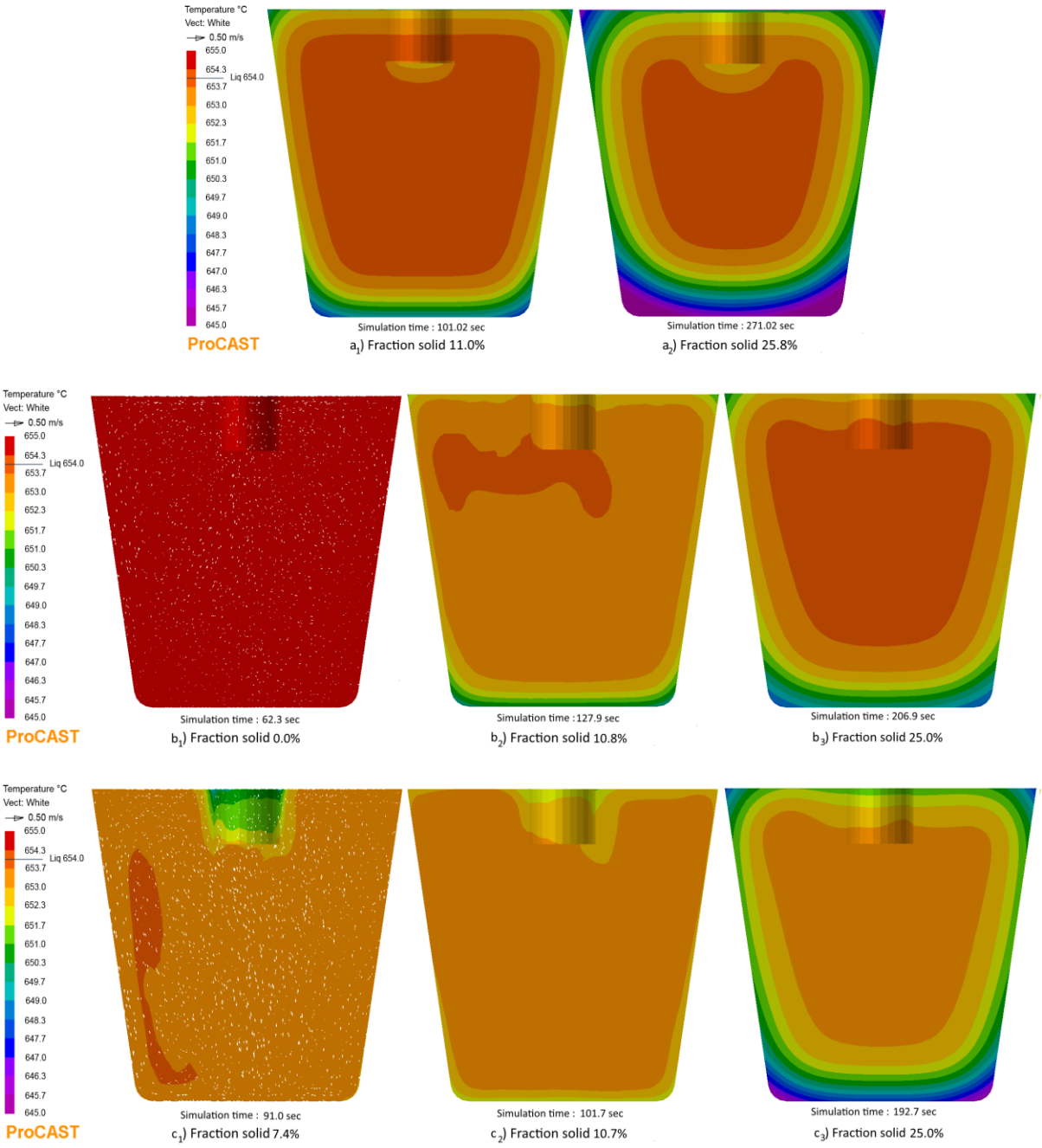

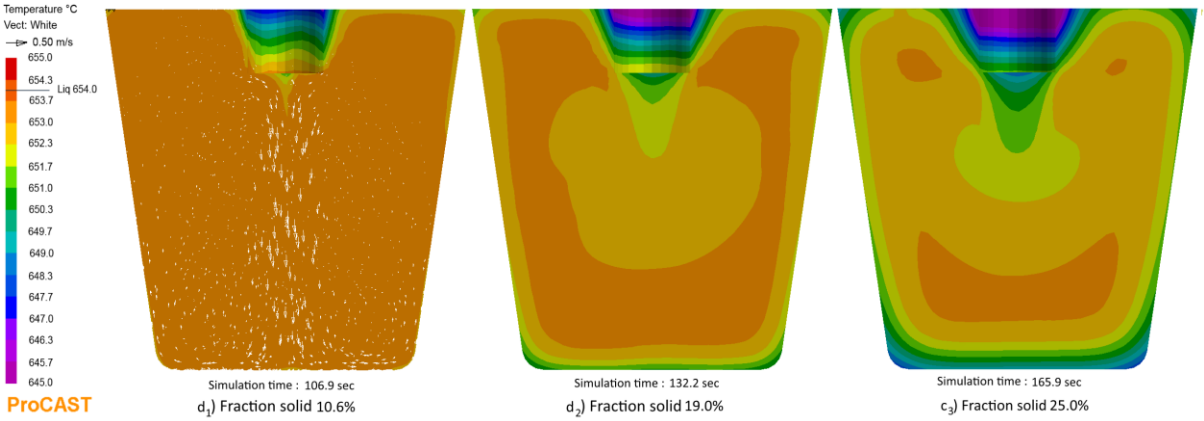

Figure 7 Simulated temperature distribution of the melt (a) without UST: (a1) 11% solid and (a2) 25% solid; (b) UST terminating when the T/C_2 reached to 660°C: (b1) when UST was terminated, (b2) 10.8% solid, and (b3) 25% solid; (c) UST terminated when T/C_2 reached the liquidus temperature at 654°C: (c1) when UST stopped, (c2) 10.8% solid, and (c3) 25% solid; and (d) UST from 694°C for 4 min: (d1)10.6% solid, (d2) 19.0% solid, and (d3) 25.0% solid. The scale bar represents the temperature from 645°C in dark purple to 655°C in red.

When removing the sonotrode from the melt at the liquidus temperature of 654°C as measured at T/C_2 (Figure 1), the solid fraction was around 7.4%, and the melt was below the liquidus temperature indicating that the solidified grains can survive remelting when UST is applied (Figure $7c_1$). Like the case terminating UST at 660°C, after removing the sonotrode, the temperature gradient increased very quickly from the outer wall to the centre as shown in Figures $7c_2$ and $7c_3$. When extending the duration of UST to 4 min, UST continually flattened the temperature gradient throughout the melt during the solidification stage (Figure $7d_1$) until the melt lost its flow capability as the solid fraction reached around 16.6% (Figure $3b_3$). Once acoustic streaming stopped, the temperature gradient then developed as indicated in Figures $7d_2$ and $7d_3$.

Figure 8 shows plots of the simulated cooling curves at T/C_2 and the temperature gradient between two points corresponding to the location of the two thermocouples in the experiments. Without UST, the temperature gradient developed and increased steadily with an increase in the cooling time to 100 seconds until the temperature reached the liquidus. When the temperature approaches the liquidus temperature, the temperature gradient decreased to almost zero within 15 seconds. Then the temperature gradient increased again as shown in Figure 8a. In comparison, the gradients when UST is applied were very unstable, and the tendency to increase the temperature gradient is much slower than that without UST as shown in Figures 8b, 8c and 8d. If UST is terminated before solidification commenced, the gradient quickly increased as revealed in Figure 8b.

The temperature gradient can be maintained at close to zero for a short period of time between the start of solidification and the time when UST is terminated at 654°C. Once the sonotrode is removed from the melt, the temperature gradient began to increase as shown in Figure 8c. Extending UST to 4 minutes maintained a low temperature gradient for about 45 seconds during the early stages of solidification. When point T/C_1 close to the side wall solidified, the

melt at this point lost its flow capacity, therefore the low temperature gradient cannot be maintained and a continuous increase of the temperature gradient occurs. It can be also observed from Figure 8 that as the time over which UST is applied is increased, the maximum temperature gradient increases indicating a relatively high rate of heat dispersion during the latter stage of solidification after UST has been stopped.

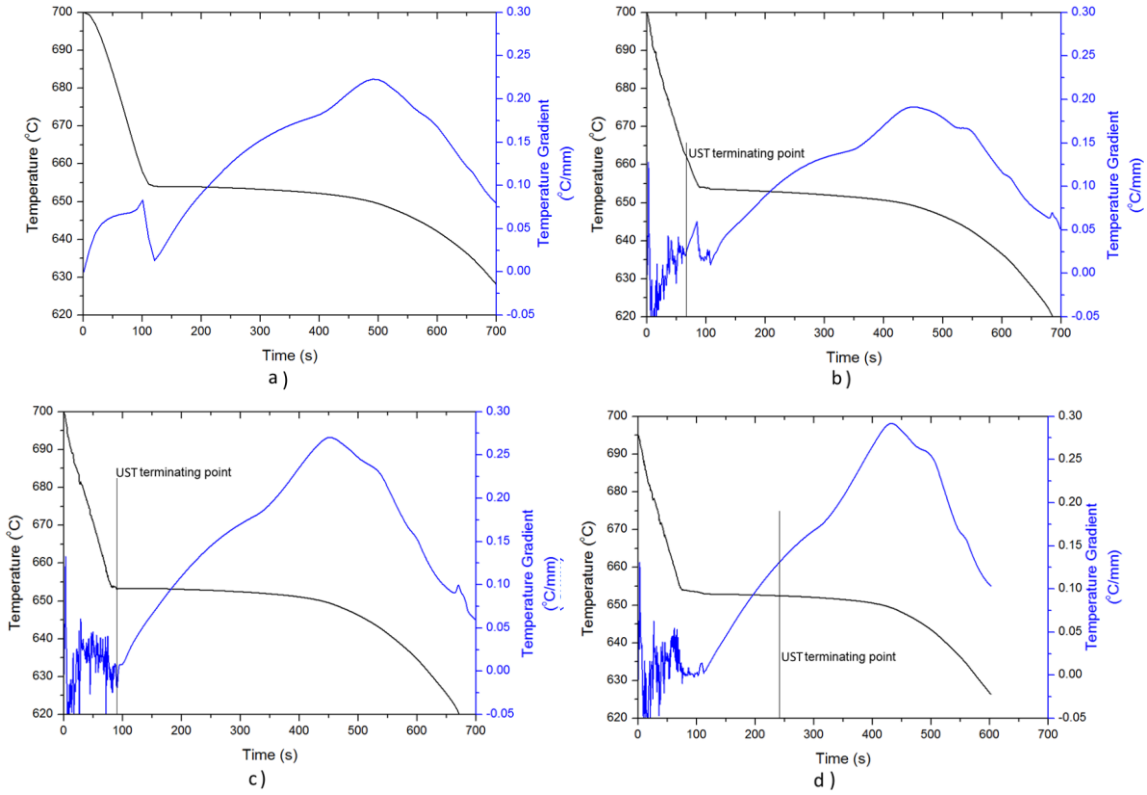

Figure 8 Simulated cooling curve for the T/C_2 and simulated temperature gredient between T/C_1 and T/C_2 (a) without UST, (b) UST terminating when the T/C_2 reached to 660°C, (c) UST terminated when T/C_2 reached the liquidus temperature at 654°C, and (d) UST from 694°C for 4 min

4.4 The mechanisms of grain refinement during UST

Ultrasonic vibrations in melts generate cavitation, the formation of cavities filled mainly with gases that dissolve into liquid metal. This is considered to be the most important factor in terms of the refinement of the as-cast grain structure [9]. Current simplified models are only capable of simulating the coupled convection flow induced by acoustic streaming and the temperature field of the melt as only part of the ultrasonic effects. So these models do not account for the cavitation effect on solidification. However, it may prove that the other ultrasonic grain refinement mechanism described in the Introduction, crystal nucleation on or near the surface of the tip of the sonotrode followed by detachment, makes a significant contribution to reducing grain size. This mechanism occurs in traditional castings when the melt is poured in a turbulent fashion into metal dies. As the melt fills the die, the cooler melt near the top of the die walls is the source of new crystals that are swept into the melt by the turbulence generating an equiaxed structure [26]. Nucleation in this region is caused by thermal undercooling which is a similar situation to the region under the sonotrode, only less vigorous. Crystals can nucleate on the

sonontrode surface, as occurs on the die walls, or in the thermally undercooled melt adjacent to this location. Only the crystals nucleated on the sonotrode (or die wall) need to be detached. The crystals nucleated near, rather than on, the sonotrode surface can be readily swept into the melt.

Detachment has been proposed to be the dominant refinement mechanism for magnetic field treatments including pulsed magnetic field (PMF), magnetic stirring in the weld pool and solidification during casting [27-29]. When a cold sonotrode is immersed into the melt, the local temperature decreases significantly generating thermal undercooling that initiates the nucleation and solidification of crystals on or near the sonotrode surface. The simulations show that the conditions produced under the sonotrode are ideal for this mechanism to operate while UST is applied.

The relatively large volume of the whole sonotrode, air cooling from the transducer end, and the good thermal conductivity of the sonotrode, result in a temperature gradient from the sonotrode tip, the body of the sonotrode, and the transducer. Therefore a relatively cold sonotrode can be maintained for the duration of the UST process, up to 4 minutes as shown in simulated results for the temperature distribution in Figure 4. It is possible that both proposed mechanisms, cavitation induced nucleation and detachment, occur together as cavitation bubbles have been observed to form and grow in recent synchrotron studies [30-31].

It is proposed that acoustic streaming generates sustained convection sufficient to create a uniform thermal environment throughout the melt. The low temperature gradient and the undercooled region beneath the colder sonotrode establishes a location for continuous nucleation, and enhances the survival of newly formed crystals as they are transported throughout the melt while UST continues to be applied. Apart from the cavitation enhanced heterogeneous nucleation mechanism, it is also possible that crystals are generated by a continuous process of nucleation on or near the surface of the sonotrode, growth of these crystals and detachment of those crystals formed directly on the radiating surface of the sonotrode. Once crystals form by either of the above mechanisms on or near the sonotrode, the new crystals are then swept into the melt by the high degree of convection caused by acoustic streaming. Thus, optimising these conditions can produce a cast structure that is fully equiaxed.

5. Conclusions

A computational model was developed to simulate the convection caused by acoustic streaming and its influence on the temperature distribution during the solidification process of an Al-2Cu alloy. The model simplified the interface between the sonotrode and melt by introducing a momentum source over a volume which equals the cavitation zone. Based on the acoustic streaming theory proposed by Lighthill, the model assumes that all the acoustic energy absorbed by the liquid is converted into turbulent motion, forming a jet under the sonotrode tip. The Navier-Stokes equations were solved using the ProCAST virtual casting software to simulate the hydrodynamic field in the melt. A detailed comparison of the experimental and the simulations results was conducted looking at the influence of the duration of ultrasonic treatment on the convective flow and the resulting temperature distribution. It was revealed

that the relatively cold sonotrode during ultrasonic treatment up to 4 minutes provides a favourable environment for crystal nucleation on or near the radiation surface of the sonotrode tip followed by detachment of grains nucleated directly on the sonotrode surface, and transportation of all grains formed on or near the sonotrode into the bulk of the melt through convective flow. The convection induced by an ultrasonic field created a low temperature gradient throughout the melt which favours the formation of an equiaxed grain structure. Therefore, it is concluded that the convective flow induced by acoustic streaming plays a critical role in promoting nucleation, growth, and transport of grains. However, it should be cautioned that convection is dampened with an increase of the solid fraction, and cannot be maintained once the solid fraction exceeds approximately 16.6%.

Acknowledgements

Authors acknowledge the financial support of the Defence Materials Technology Centre, which was established and is supported by the Australian Government's Defence Future Capability Technology Centre (DFCTC) initiative and ARC Discovery grant DP140100702. The simulation work was done under the collaboration of the DMTC, of which The University of Queensland is a member and the Pacific ESI is an associate.

References

1. J. Wannasin, R. Canyook, S. Wisutmethangoon, M. C. Flemings, Grain refinement behavior of an aluminum alloy by inoculation and dynamic nucleation, Acta Mater. 2013, 61, 3897.
2. D. Liang, J. Sun, T. Liu, Q. Zhai, G. Wang, D.H. StJohn, H. Dong, and H Zhong, Enhanced Heterogeneous Nucleation by Pulsed Magneto-Oscillation Treatment of Liquid Aluminum Containing Al3Ti1B Additions,
3. Z. Fan, G. Liu, Solidification behaviour of AZ91D alloy under intensive forced convection in the RDC process, Acta Mater. 2005, 53, 4345
4. X. Jian, T. T. Meek, Q. Han, Refinement of eutectic silicon phase of aluminum A356 alloy using high-intensity ultrasonic vibration, Scripta Mater. 2006, 54, 893.
5. G.I. Eskin, D.G. Eskin, Ultrasonic Treatment of Light Alloy Melts, 2nd Edition, CRC Press.
6. O.V. Abramov, Ultrasound in Liquid and Solid Metals, CRC Press, Boca Raton, FL, 1994.
7. T.V. Atamanenko, D.G. Eskin, L. Zhang, and L. Katgerman, Criteria of Grain Refinement Induced by Ultrasonic Melt Treatment of Aluminium Alloys Containing Zr and Ti, Metallurgical and Materials Transactions, 41A 2056-2066
8. J. Mi, D. Tan, T. L. Lee, Metallurgical and Materials Transactions B, 2015, 46, 1615.
9. Dmitry G. Eskin, Ultrasonic Melt Processing: Achievements and Challenges, Materials Science Forum 828-829: 112-118
10. S. Jia, L. Nastac, The Influence of Ultrasonic Stirring on the Solidification Microstructure and Mechanical Properties of A356 Alloy, Chemical and Materials Engineering 1 (3): 69-73, 2013
11. S.K. Bhangu, M. Ashokkumar, and J. Lee, Ultrasound Assisted Crystallization of Paracetamol: Crystal Size Distribution and Polymorph Control, Crystal Growth and Dessign, 2016, 16 (4), pp 1934–1941
12. J. B. Ferguson, B.F. Schultz, K. Cho and P. K. Rohatgi, Correlation *vs.* Causation: The Effects of Ultrasonic Melt Treatment on Cast Metal Grain Size, Metals 2014, 4, 477-489
13. G. Wang, M.S. Dargusch, M. Qian, D.G. Eskin, D.H. StJohn, Journal of Crystal Growth, 2014, 408, 119.
14. Martin Wiklund, Roy Green, and Mathias Ohlin, Acoustofluidics 14: Applications of acoustic streaming in microfluidic devices Lab Chip, 2012, 12, 2438–2451
15. Nyborg, W. L. (1958). Acoustic Streaming near a Boundary, Journal of the Acoustical Society of America 30(4): 329-339.
16. Tjotta, S. (1999). Theoretical Investigation of Heat and Streaming Generated by High Intensity Ultrasound. Acustica **85**: 780-787.
17. Riley, N. (1998). Acoustic streaming. Theoretical and Computational Fluid Dynamics **10**: 349-356.

18 M.B. Dentry, L.Y. Yeo, J.R. Friend, Frequency effects on the scale and behavior of acoustic streaming, Physical Review E89, 013203 (2014)
19 F. J. Trujillo and K. Knoerzer, CFD Modelling Of The Acoustic Streaming Induced By An Ultrasonic Horn Reactor, Seventh International Conference on CFD in the Minerals and Process Industries, CSIRO, Melbourne, Australia 9-11 December 2009
20 H. Lei, D. Henry, H. Ben Hadid, Numerical study of the influence of a longitudinal sound field on natural convection in a cavity, International Journal of Heat and Mass Transfer 49 (2006) 3601–3616
21 W. Dridi, D. Henry, H. Ben Hadid, Influence of acoustic streaming on the stability of melt flows in horizontal Bridgman configurations, Journal of Crystal Growth 310 (2008) 1546–1551
22. J. Lighthill, Acoustic streaming, Journal of Sound and Vibration (1978) **61**(3): 391-418.
23. ESI Group, ProCAST User Manual, Paris France, 2016.
24. A Kumar, T. Kumaresan, A. B. Pandit, J. B. Joshi, Characterization of flow phenomena induced by ultrasonic horn, Chemical Engineering Science 61 (2006) 7410 – 7420
25. Yasuo Ishiwata, Sergey Komarov and Yoshihiro Takeda, Investigation of Acoustic Streaming in Aluminum Melts Exposed to High-Intensity Ultrasonic Irradiation, 13th International Conference on Aluminum Alloys (ICAA13) Edited by: Hasso Weiland, Anthony D. Rollett, William A. Cassada TMS (The Minerals, Metals & Materials Society), 2012
26. J.E.C. Hutt and D.H. StJohn, The origins of the equiaxed zone: Review of theoretical and experimental work, International Journal of Cast Metals Research, 11 (1998) 1, 13-22
27. X. Ma, Y. Li, and Y. Yang, Grain refinement effect of pulsed magnetic field on solidified microstructure of superalloy IN718, *Journal of Materials Research* 24 (2009) 3174-3181
28. M.G. Mousavi, M.J.M. Hermans, I.M. Richardson, and G. den Ouden, Grain refinement due to grain detachment in electromagnetically stirred AA7020 welds, Science and Technology of Welding and Joining 8 (2003) 309-312 DOI: http://dx.doi.org/10.1179/136217103225005462
29. Y.X. Wang, X.Q. Zeng, and W.J. Ding, Alan A. Luo and Anil K. Sachdev, Grain Refinement of AZ31 Magnesium Alloy by Titanium and Low-Frequency Electromagnetic Casting, Metallurgical and Materials Transactions A 38 (2007) 1358-1366
30. D. Tan, T.L. Lee, J.C. Khong, T. Connolley, K. Fezzaa, and J. Mi, High-Speed Synchrotron X-ray Imaging Studies of the Ultrasound Shockwave and Enhanced Flow during Metal Solidification Processes, Metallurgical And Materials Transactions 46A (2015) 2851-2861
31. W.W. Xu, I. Tzanakis, P. Srirangam, W.U. Mirihanage, D.G. Eskin, A.J. Bodey, P.D. Lee, Synchrotron quantification of ultrasound cavitation and bubble dynamics in Al–10Cu melts, Ultrasonics Sonochemistry 31 (2016) 355–361